Development of Graphene Nano-platelet Ink for High Voltage Flexible Dye Sensitized Solar Cells with Cobalt Complex Electrolytes.

*J. A. Baker†‡ C. Worsley†, H. K.H. Lee†, R.N. Clark†, W.C, Tsoi†, G. Williams†, D. A. Worsley†, D .T Gethin‡, T. M. Watson†**

†SPECIFIC, College of Engineering, Swansea University Bay Campus, Swansea, SA1 8EN, U.K.

‡WCPC, College of Engineering, Swansea University Bay Campus, Swansea, SA1 8EN, U.K.

*corresponding author,

KEYWORDS

Graphene ink, printing, dye sensitized solar cells, roll to roll, flexible electronics

ABSTRACT

Graphene nanoparticles have been subject to intensive investigation as a replacement for platinum as the catalyst in dye sensitized solar cells (DSCs), but few of these investigations examine the application for flexible cells with deposition processes suitable for industrial fabrication. This work introduces a transparent water based graphene ink that can be deposited via flexographic, slot die and K-bar coating and dried rapidly at less than 110ºC making it particularly suitable for roll to roll deposition on plastic substrates. By optimizing the binder loading the surface area of the deposited ink can be maximised whilst maintaining the rheological properties of the ink necessary for deposition by a wide range of techniques. This ink has application as a catalyst for dye sensitized solar cells utilizing cobalt complex electrolytes with efficiency of over 6 % and a V_{oc} of 0.89 V at 1 sun demonstrated. A flexible DSC with a printed catalyst and cobalt redox mediator is reported, with efficiency of over 6.0 % and V_{oc} of 0.6 V at 800 lux.

1. Introduction

Solution processed flexible solar cells which have lower embodied energy[1] than conventional silicon based solar cells[2] are the focus of much academic research, with the aim of harnessing solar energy at reduced cost compared to the incumbent silicon technology. Of all the solution processed solar cell technologies the DSC is the most industrially advanced, with modules available commercially[3] and lifetimes exceeding 25,000 hours in full illumination[4].

Although DSC research often focusses on outdoor performance under AM1.5 irradiation, there is great potential for these devices to be used indoor where the spectra is suited for higher bandgap devices harvesting light at lower wavelengths[5]. The requirements of indoor photovoltaics (PV) have been growing rapidly thanks to the development of the small scale and wirelessly connected Internet of Things (IoT); necessary for making smart homes or offices possible[6–8]. For design reasons such applications may require flexible PV as a power source. Here, we tested flexible DSC under low light environments for indoor applications. The unit used for light intensity, lux, is normally used as an indoor light level indicator. A typical office environment is around 300-500 lux, whilst supermarket environments are typically brighter.

The DSC owes its success to a high surface area nano-crystalline TiO_2[9] layer which maximises dye adsorption, leading to higher potential photocurrent. During operation of the cell the dye oxidises and must be regenerated, this is usually achieved using an I^-/I_3^- redox mediator[10–12]. The redox potential of the iodide couple is quite low (0.35 V vs SHE)[13] which limits the open circuit voltage to around 0.75 V. In order to increase the V_{oc} and therefore the photo conversion efficiency (PCE), cobalt redox couples[14,15] have been used. The cobalt couple is a single electron transfer reaction in contrast to the two electron transfer reaction of iodide. Cobalt redox couples have a higher redox potential (0.56 V vs SHE) compared with iodide, enabling open circuit voltages of over 0.9 V[16] and PCE of over 13 %[17].

Platinum is most commonly used to catalyse the redox reaction in DSCs. Due to the high cost of platinum a wide range of other catalysts have been investigated as replacements including carbides[18,19], oxides[20,21], polymers[22] and carbon nanomaterials[23–25]. Carbon based catalysts have been demonstrated to be stable in liquid electrolyte DSCs [26,27] making them a good candidate to replace platinum. However carbon materials typically demonstrate reduced electrochemical performance [28–33] in an iodide based electrolyte. Conversely GNP powders have been shown to be excellent catalysts for the cobalt redox reaction[34–39] both in terms of electrochemical performance[37] and electrochemical stability[39–41].

A DSC can be manufactured on both rigid and flexible substrates. A glass based DSC with the architecture shown in Figure 1a has the advantage that both substrates can withstand processing temperatures of over 550ºC, enabling both the deposition of the mesoporous TiO_2 layer and the catalyst layer at high temperature. Due to its rigid nature a glass based DSC cannot be manufactured using roll processing and the final product is brittle and cannot easily be incorporated into flexible electronic applications. By incorporating a metal foil with an ITO-PET top sheet into the architecture, as shown in Figure 1b, the DSC can be manufactured by roll to roll printing technologies. The metal foil enables the mesoporous TiO_2 to be sintered at 550ºC but the ITO-PET limits the temperature of the catalyst deposition to < 150ºC[42]. In most cases titanium is used as the metal foil substrate due to its excellent corrosion resistance towards the liquid electrolyte[42–46] although the stability of other metals have been investigated[47]. The opaque nature of the metal foil in the flexible cell requires the DSC to be illuminated through the ITO-PET, catalyst and electrolyte and therefore reverse illuminated flexible cells typically have lower photocurrents than their forward illuminated counterparts[48].

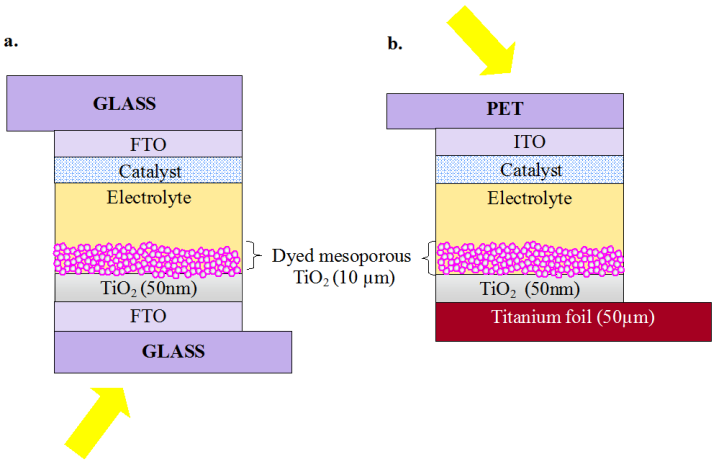

Figure 1(a) glass based DSC architecture, **(b)**, metal foil reverse illumination DSC architecture.

In order to deposit the nanoparticle platinum catalyst onto ITO-PET, plasma sputtering is used which is a vacuum based technology with high capital cost associated with the equipment and the platinum target[43]. This has led to GNP research as a replacement catalyst for sputtered platinum on ITO-PET substrates[29]. Although there have been many papers discussing the merits of GNP catalysts[29,36,49] very few have focussed on developing inks which can be deposited by industrial printing methods[31,50] whilst also achieving the transparency[37] and processing requirements to make them suitable for use in flexible DSCs manufactured by roll to roll technologies.

When applied without a binder the GNPs are poorly adhered to the surface of the counter electrode, as shown in Table S1, and can be easily damaged during the assembly of the DSC[51]. It is also likely that poor adhesion will limit the lifetime of the cell, since when the GNP detaches from the counter electrode the catalyst performance will be reduced and recombination will be increased (as the GNP can migrate and catalyse the redox reaction at the photo electrode rather than the counter electrode). Binders have been used to develop GNP pastes, which have the required adhesive properties, but the resultant films are opaque and require high temperature treatments, limiting the use of these films on

flexible conductive substrates such as ITO-PET[36]. Kavan developed a hybrid material of reduced graphene oxide (rGO) and GNP powder which had superior adhesion to GNP powder on its own, but this material required a high temperature treatment unsuitable for plastic substrates[52].

This work develops and characterises a GNP ink capable of being deposited by a variety of printing and coating techniques, without the requirement of high temperature processing (< 150 ºC). Specific surface area was optimised to ensure that the ink maintained good catalytic behaviour at the low ink loadings necessary for semi-transparent catalysts, essential for a flexible opaque metal substrate DSC[48].

2. Experimental

2.1 Ink production and characterisation

To make the inks sodium carboxymethylcellulose (CMC) was used as a binder, 419338 Aldrich, average M_w ~700,000. Isopropanol (IPA) was purchased from Sigma Aldrich. Graphene nanoplatelet (GNP) powder was obtained from Haydale with the trade name XG-C750 (XGSciences). The GNP powder was mixed with IPA in an ultrasonic bath for 30 minutes to reduce agglomeration. To make the ink, 7 ml of CMC solution (in de-ionized water) was slowly added whilst stirring with a magnetic stirrer. To ensure a good dispersion of the CMC within the ink a Bandelin Sonoplus 3100 ultrasonic homogeniser was used with a 3 mm tip, probe settings were 20 kHz, pulse time of 0.5 s on 0.5 s off.

AFM samples were prepared by sonicating the GNP powder in IPA (0.1 mg/ml) for 30 minutes before dropping onto a cleaned silicon wafer and drying, images were obtained using a JPK instrument Nanowizard 3 AFM in contact mode with a line rate of 0.9 Hz. First order polynomial fitting was used to level scans with an X-Y resolution of 1.94 nm. The Z piezo height was 5 µm and Z resolution 0.4 pm. SEM images were taken using a Hitachi FEG-SEM, with a 15 kV accelerating voltage. Nitrogen

adsorption measurements were taken using a Micromeritics Tristar Surface analyser, degassing time was a minimum of 4 hours at 0.02 mBar for GNP powders. When performing surface analysis of inks degassing was not carried out in order to evaluate the surface area in the as deposited state. Transmission measurements were measured using a Perkin Elmer Lambda 750 UV-Vis spectrophotometer. Isothermal cone and plate viscosity measurements were carried out at 25°C using a Malvern Bohlin Gemini HR Nano Rheometer utilising air bearing technology to ensure accurate measurements at low torque. Surface tension measurements were carried out using a Fibrodat 1100 dynamic 65 contact angle measurement system, with an 8 µl pumped drop.

The adhesion of the catalyst was tested by applying Magic Tape™ (3M) to the catalyst deposited onto an ITO-PET substrate. This was then pressed into place using a force of 20 kg/ cm^2 (produced by a MSK-110 hydraulic machine). The tape was then peeled off the substrate at 90º. Transmission of the catalyst layer at 550 nm was measured before and after the test to determine the percentage of catalyst removed by the adhesion test.

2.2 Device fabrication and testing

Device architectures for glass and flexible metal based cells are shown in Figure 1. A compact TiO_2 layer was deposited onto either; TEC 7 FTO glass or 50 µm thick Grade 2 titanium foil, by spraying 0.2 M titanium di-isopropoxide bis(acetylacetonate) in isopropanol at 300ºC and then sintering at 550°C for 30 minutes. The mesoporous TiO_2 layer was prepared by depositing a 5 µm layer of Dyesol 18-NRT paste on top of the compact TiO_2 followed by an additional mesoporous TiO_2 layer (5 µm layer of Dyesol WERO 0-2) for improved light scattering. The bi-layer paste was then sintered at 550ºC for 30 min. The whole TiO_2 electrode was immersed in $TiCl_4$ for 30 min at 80ºC and re-sintered at 550º before being dyed in 0.2 mM D35 in ethanol overnight. The counter electrode was prepared using TEC 7 FTO glass with either sputtered platinum deposited using a Quorum 150TES, current setting 30 mA, 0.1mm

Pt target to a thickness of 2 nm, or GNP ink deposited by spin coating at 2000 rpm for 45 seconds and drying at 110ºC for 10 minutes. For the flexible DSC the GNP ink was deposited using an RK printer, speed 3 and K-bar (no. 0) coating onto 50 Ω/□ ITO-PET and dried at 110°C for 10 minutes. For glass cells a 25 µm Surlyn™ spacer was used to separate the working electrode from the counter electrode and then electrolyte (0.22 M $Co(bpy)_3$ $(B(CN_4)_2$, 0.05 M $Co(bpy)_3$ $(B(CN)_4)_3$, 0.1 M $LiClO_4$, 0.2 M 4 tert- butyl pyridine) was introduced by a syringe pump through a pre-drilled hole. Cobalt complexes were supplied by Dyenamo. Flexible cells were fabricated on 50 µm thick titanium foil, with compact TiO_2 layer as previously described. Due to the already reflective nature of the titanium foil a single 10 µm 18NRT layer was used as the mesoporous TiO_2 which was then subject to $TiCl_4$ treatment as described previously. The working electrode was sealed to the ITO-PET substrate using 60 µm Surlyn gasket. In all cases 1 cm^2 cells were manufactured and masked before current voltage characteristics were measured under 1000 W/m^2, AM 1.5 illumination using a Sol3A solar simulator calibrated using a KG5 filtered silicon reference cell. Low light J-V measurements were taken using a Keithley 2400 source meter under a series of fluorescent lamps, Osram L18W/827. A luxmeter, LX-1330B, was used to measure the lux level of the fluorescence lamps. The light intensity calibration of the fluorescent lamps was performed by a Thorlabs PM100D power and an energy meter using a Thorlabs S401C high-sensitivity thermal sensor

2.3 Electrochemical impedance testing

Symmetrical ‘dummy’ cells (whereby two counter electrodes are sealed together) were sealed with 60 µm Surlyn™ and filled with the same cobalt electrolyte used for the DSC manufacture. Electrochemical impedance (EIS) measurements were taken using a Gamry Potentiostat from 400,000 Hz to 0.1 Hz under a bias potential of 0 V and an alternating component ramped at 10 mV/s.

3. Results and Discussion

A particulate ink is typically comprised of an active material (GNP), carrier liquid, long chain polymer binder, solvent for the binder and surfactants as necessary to reduce the surface tension and ensure adequate wetting of the substrate. The role of the carrier liquid is to suspend the GNP particles and allow them to be fully dispersed before mixing with the binder. Prior to making the ink the GNP powder was characterised by AFM, Figure 2a presents the flake thickness, demonstrating that the majority of GNP flakes had a thickness of < 2 nm, a typical AFM scan is presented in Figure S1. The bimodal distribution of flake thickness is most likely due to GNP agglomeration, Figure 2b shows a GNP agglomerate of multiple flakes which have not been completely dispersed by sonication.

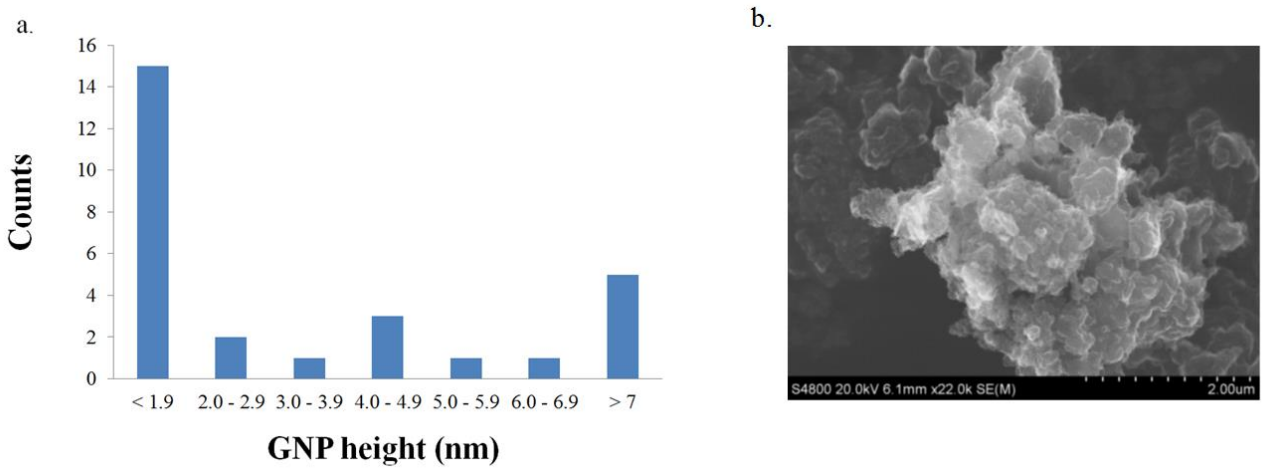

Figure 2 (a) Thickness of dispersed graphene flakes, measured by AFM, **(b)** SEM image of GNP agglomerate.

GNP thicknesses of < 2 nm thick, give an interlayer spacing of 0.34 nm[53], which corresponds to flakes with < 6 graphene layers. Nitrogen adsorption can also determine average GNP thickness, at least 70 mg of GNP powder was analysed in each measurement and the BET surface area was calculated to be 668 (± 7) m^2 / g. This corresponds to an average GNP thickness of < 4 graphene layers, supporting the hypothesis that the sample contains some agglomerates. X-ray photoelectron (XPS) analysis of the

GNP powder was performed in previous work[12], indicating that the GNPs had 4.3 at. % O (1s) and 0.98 at. % N (1s) functionalization.

When making an ink the GNPs only need to be suspended in the carrier liquid for a short time, since long term suspension is provided by the binder, this allows isopropanol (IPA) to be used rather than benzo benzoate or N-methylpyrrolidone which whilst showing better suspension performance[54] than IPA have higher toxicity[55,56] and therefore are less suited to commercial manufacture. IPA has a lower surface tension than water and when added to water based solutions will reduce the surface tension, as shown in Figure 3a (where IPA is added to a 0.15 wt.% CMC solution), therefore the wetting can be improved without the need for further surfactants.

To enable deposition by a range of coating techniques, the viscosity of the ink must be at least 20 mPas[28] . To enable maximum catalytic performance the viscosity must be maximised with the minimum amount of inert binder material, since a binder can reduce catalytic activity by reducing the surface area of the ink, as shown in Figure 3c. The CMC binder in H_2O exhibits non-Newtonian rheological behaviour, reducing in viscosity with increasing shear rate as the polymer chains align. Because CMC binder solution is not soluble in IPA, adding IPA to CMC binder solution causes a gelling effect, shown in Figure 3a, beneficially doubling the viscosity without addition of further binders. In order to ensure complete dispersion of the GNP particles within the CMC binder solution the ink was mixed with an ultrasonic probe. The behaviour of the ink becomes more Newtonian after mixing with the probe, as seen in Figure 3b, due to alignment of the polymer chains, however the viscosity at 1000 s^{-1} remains unchanged.

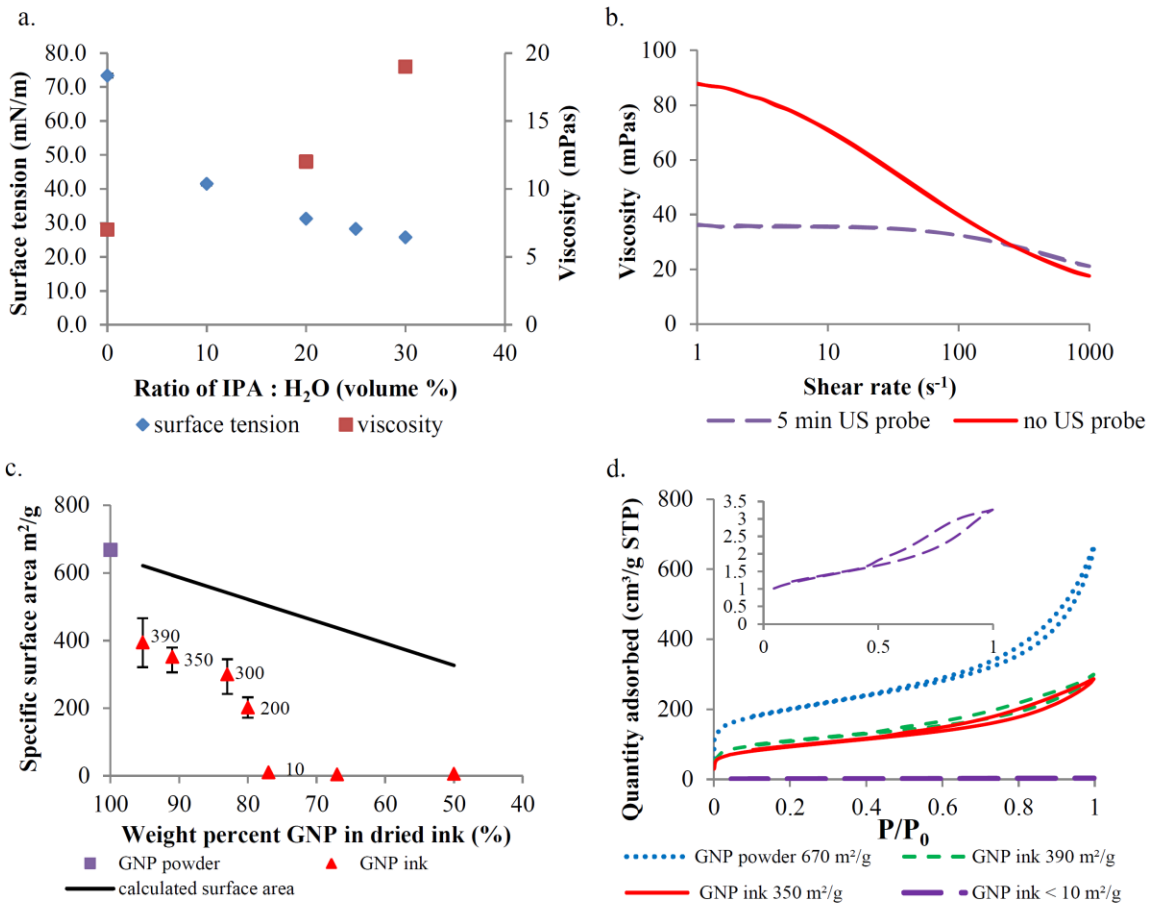

Figure 3 (a) Effect of ratio of IPA: H_2O (volume %) upon the surface tension and viscosity (at a shear rate of 1000 s^{-1}) of 0.15 wt. % CMC binder solution. **(b)** Effect of mixing with an ultrasonic probe on the viscosity of GNP ink (composition 0.15 g CMC, 3 ml IPA, 7 ml H_2O, 0.015 g GNP. **(c)** Effect of CMC binder content on BET surface area of dried ink, markers are an average of at least three results, error bars represent minimum and maximum values. Data values given to 2 significant figures **(d)** Comparison of nitrogen adsorption isotherms (77 K) for GNP powder and inks with surface areas, inset GNP ink surface area < 10 m^2/g, with enlarged y-axis scale.

Although the CMC binder is necessary to improve the rheological properties of the ink and to provide adhesion of the GNP to the substrate surface it can reduce the catalytic activity of the GNPs by

blocking active sites on their surface; surface area has been shown to be a key characteristic for determining the catalytic activity of carbon nanomaterials in a DSC[28,57–59]. In order to understand the extent to which the CMC binder blocks the GNP active sites and reduces the surface area, a number of different inks were produced with different GNP:CMC ratios whilst keeping all constituents of the ink constant. The BET surface area of these inks is presented in Figure 3c and representative isotherms of 3 inks with surface areas of 390 m^2/g, 350 m^2/g and < 10 m^2/g are compared with GNP powder in Figure 3d.

The surface area of the ink (SA_{ink}) was predicted using a CMC binder specific surface area (SA_B) value of 1 m^2/g and the previously measured specific surface area of the GNP powder (SA_{gnp}). This allowed the SA_{ink} to be predicted using Equation 1, where B is the mass ratio of CMC binder to GNP in the dried ink. The results are plotted in Figure 3c.

$$SA_{ink} = (S_{AB} \times B) + (SA_{GNP} \times (1-B)) \qquad \text{Equation 1}$$

The calculated surface area is much higher than the measured surface area suggesting the CMC binder is blocking some of the active sites as it wraps around the graphene. Figure 3d shows that regardless of surface area they all display type 4 iostherms, enabling a valid BET measurement. For the GNP powder the near vertical increase in gas adsorbed at P/P_0 approaching 1 is characteristic of macropores > 50 nm in size[60] this is likely due to pores created between individual GNP powders within the GNP agglomerates. This affect is less marked in the inks indicating that the ink making process has reduced individual GNP agglomeration.

The as received GNP powder has a BET surface area of 670 m^2 / g, however when an ink is made with 95 wt. % GNP the surface area reduces significantly to 390 m^2/g, as shown in Figure 3c. Reducing the

GNP content further to 91 wt. % causes a small reduction to the surface area from 390 m^2/g to 350 m^2/g but made a significant improvement to the GNP adhesion to the substrate surface. Inks with 91 wt% GNP and a surface area of 350 m^2/g were adhered enough to the substrate such that after an adhesion tape test the transmission was almost unchanged (Table S1 shows the results of the adhesion test) indicating that less than 10 % of the ink was removed during the test. This was a significant improvement in adhesion compared to the ink which had 95 wt % GNP content where 50 % of the ink was removed during this test.

Further reductions in GNP content (to < 80 wt.%) caused a total reduction in surface area (to less than 10 m^2/g) and this coincides with complete coating of the GNP powder with CMC such that the film could be removed from the substrate in one piece. The optimum GNP content was determined to be 91 wt. %, based on surface area measurements and adhesion performance and therefore this ink with surface area 350 m^2/g was used for ongoing tests. The viscosity of this ink is shown in Figure 3b, meeting the 20 mPas requirement for deposition by slot die and flexographic printing, whilst maximising specific surface area. Pictures and schematics of the slot die, flexographic and K-bar printing processes are given in Figures S2 -S4.

Having fixed the ink composition the loading of the deposited ink was controlled by ink metering during the deposition process. Ink loading was related to the transmission of the catalytic film at 550 nm (T_{550}) to allow comparison with the transmission of sputtered platinum (T_{550} = 75 %), which is particularly important in reverse illuminated cells. For bar coating onto ITO-PET the loading was controlled by changing the wire diameter of the wound bar, bar 0 (wire diameter 50 µm) gave an ink loading which corresponded to a film transmission of 85 %, whilst bar 1 (wire diameter 80 µm) gave a film transmission of 75 %.

In order to confirm the catalytic activity of the GNP ink towards the redox couple, the charge transfer resistance (R_{ct}) of symmetrical cells was measured at open circuit by EIS, these cells had two counter electrodes on either side of the cobalt electrolyte as described in the experimental section. The performance of the cathode can then be assessed without interference from the TiO_2[36,51,52,61,62]. The target R_{ct} at the counter electrode can be related to the exchange current density (j_0) by Equation 2, where F is Faraday's constant, T is the temperature in Kelvin and R is the ideal gas constant.

$$R_{ct} = RT/(j_0nF) \qquad \text{Equation 2}$$

To avoid all losses due to charge transfer resistance, the exchange current density should be greater than the short circuit current density (J_{sc}) of the DSC so that the rate of reduction at the counter electrode does not limit the rate of dye regeneration at the photo-electrode. This allows the target R_{ct} to be calculated for a DSC under different conditions (illumination intensity and direction of illumination through the cell). For a high efficiency DSC with the architecture shown in Figure 1a, a J_{sc} of 20 mA/cm^2 was used in the calculation (298 K, 1000 W/m^2), in the same conditions a reverse illuminated metal foil DSC, utilising materials suitable for mass production and with architecture shown in Figure 1b, was anticipated to have a J_{sc} of 7 mA/cm^2.

The cobalt redox couple is only a one electron transfer reaction (n=1) and therefore the ideal R_{ct} is higher than for iodide based electrolytes where n=2. For low light applications with illuminations equivalent to 100 W/m^2 a reverse illuminated flexible DSC with cobalt electrolytes need an R_{ct} of only 37 Ω/cm^2, whereas for high efficiency applications in full sunlight an R_{ct} of 1.2 Ω/cm^2 is ideal. The charge transfer of the GNP ink is investigated at two different ink loadings T_{550} = 75 % which is equivalent to sputtered platinum and a lower loading T_{550} = 85 %. The impedance characteristics of the GNP ink are compared with sputtered platinum and GNP powder in Figure 4a and b. Typically dummy

cells exhibit a series resistance (R_s) which is a combination of the resistance of the conducting substrate, connections and the electrolyte (the substrate is usually the most significant part of the R_s). They also exhibit a charge transfer resistance (R_{ct}) which was attributed to the $Co(bpy)_3^{3+/2+}$ reaction and will reduce with increased loading of catalyst. Thirdly a diffusion resistance was attributed to the diffusion of ions across the electrode gap, which was modelled using a Warburg diffusion element (W_s) [63], since the dummy cells had the same geometry and electrolyte concentration this diffusion resistance was similar in all cells as seen in Figure 4a, b and Table 1. The sputtered platinum and GNP powder were modelled using a traditional Randles circuit[63] shown in Figure 4c. Because a symmetrical cell was used to measure the charge transfer resistance the modelled resistance was twice the resistance at a single electrode.

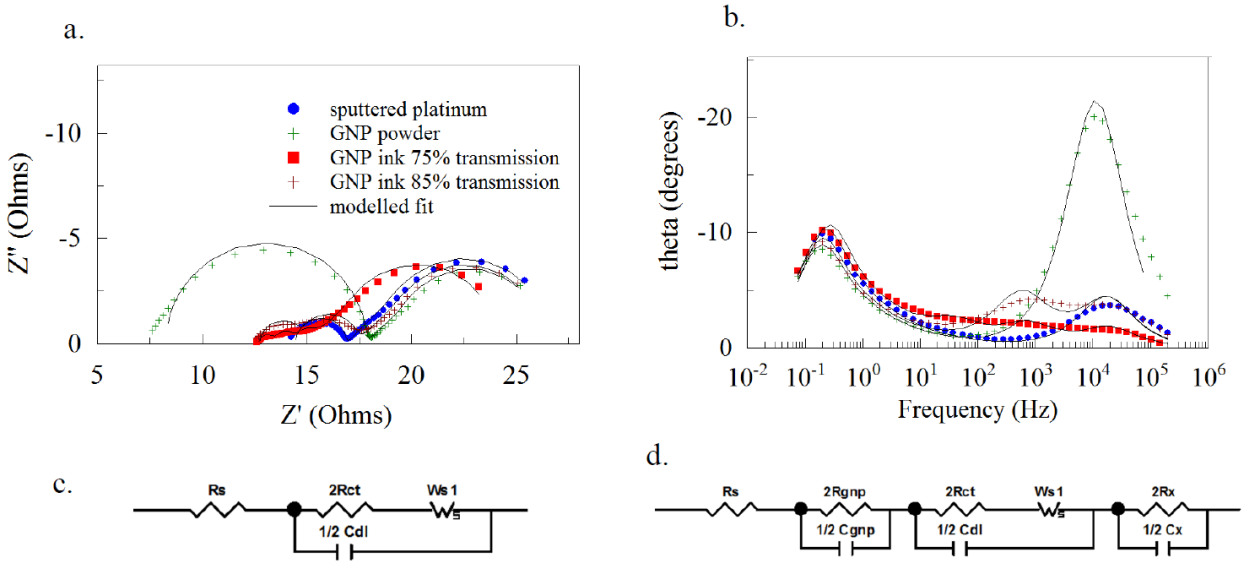

Figure 4 (a) Nyquist plot of impedance characteristics of GNP inks at two ink loadings (determined by ink transmission), compared with GNP powder and sputtered platinum. All tests were performed at open circuit potential. **(b)** Plot of phase angle versus frequency of the data presented in Figure 4a. **(c)** Equivalent (Randles) circuit for platinum and GNP powder. **(d)** Equivalent circuit for graphene ink,

As seen in Table 1, the GNP powder had a higher R_{ct} (4.7 Ω/ cm^2) than either the ink or the platinum, due to the poor adherence and distribution of the GNPs to the substrate. However the double layer capacitance (C_{dl}) of the GNP powder is the lowest of all the catalysts indicating that GNPs have fast kinetics with respect to the $Co(bpy)_3^{3+/2+}$ reaction. The GNP ink catalysts exhibit different impedance characteristics compared to the platinum and GNP powder catalysts and the data does not fit using a traditional Randles circuit (Figure 4d). The GNP inks have been modelled using the equivalent circuit in Figure 4c, as there is an extra high frequency curve, previously seen in literature for ink based catalysts[12,61]. This high frequency curve is described by the element R_{gnp} representing the contact resistance of the GNP ink with the FTO substrate as proposed by Baker et. al.[12].

In addition to the extra high frequency curve the mid frequency curve was flattened and it was hypothesised that the presence of the CMC binder wrapping around the GNPs caused them to have variable charge transfer resistances, with some areas with sites very open to easy charge transfer resistance and some areas with a lower frequency of charge transfer. The CMC binder was not active towards the $Co(bpy)_3^{3+/2+}$ reaction, confirmed by EIS of a symmetrical cell manufactured with an ink containing only CMC, as shown in Figure S5. To represent the variable R_{ct} two types of charge transfer (R_x and R_{ct}) were modelled with R_{ct} representing charge transfer directly onto the GNP and R_x representing charge transfer onto a partially blocked site.

The total charge transfer resistance of the GNP ink equals the sum of R_{gnp}, R_{ct} and R_x which for a GNP ink with transmission,T_{550} = 85 %, is 2.6 Ω/cm^2, this is suitable for all but the most demanding scenarios. When the ink loading was increased (leading to a reduction in transmission, T_{550} = 75 %, the total R_{ct} reduced to 1.3 Ω/ cm^2, equivalent to sputtered platinum as seen in Table 1. Therefore for forward illuminated DSCs the ink loading should be targeted to be at least T_{550} = 75 % whereas for reverse illuminated cells a lower ink loading will result in higher efficiency cells, less light will be

blocked by the catalyst and with a reduced current the higher R_{ct} will not limit catalytic performance. In addition to performance improvements, optimising catalyst loading to the application enables the cost of the catalyst to be minimised by ensuring that minimum amount of catalyst is used.

Table 1 – Modelled impedance characteristics for different catalysts, with $Co(bpy)_3^{3+/2+}$ electrolyte.

Catalyst	R_s(Ω)	R_{ct}(Ω)	Ws R(Ω)	C_{dl} (μF)	R_{gnp} (Ω)	C_{Gnp} (μF)	R_x (Ω)	C_{dlx} (F)	Total R_{ct} (Ω)
Platinum	14.4	1.4	9.7	8.4	n/a	n/a	n/a	n/a	1.4
GNP	8.2	4.7	8.5	4.4	n/a	n/a	n/a	n/a	4.7
GNP ink T = 75 %	12.7	0.4	9.0	24.0	0.5	175	0.4	0.024	1.3
GNP ink T = 85 %	12.7	1.0	8.9	8.0	1.0	35	0.6	0.0026	2.6

A lower contact resistance (R_{gnp}) was measured for the GNP ink catalyst with a higher loading, this is in agreement with previous work[12], due to an increased contact area of the GNP ink with the substrate.

The electrocatalytic activity of the GNP ink was investigated further by cyclic voltammetry (CV). The cyclic voltammogram, Figure S6a, shows the single electron transfer of the cobalt redox reaction. A

pair of peaks are observed for both the platinum and GNP ink catalysts with peak separations of 0.27 V and 0.25 V respectively, indicating high electrochemical activity for the Co^{3+} reduction reaction. The current limitation (J_{lim}) of the system, controlled by the mass transport of the cobalt electrolyte, is shown according to Equation 3, where n = 1 is the number of electrons, F is the Faraday constant, C is the concentration of the transport limiting Co^{3+} ions (50 mM) , D is the diffusion coefficient and δ is the distance between electrodes in a dummy cell (60 μm).

$$J_{lim} = 2nFCD/\delta \qquad \text{Equation 3}$$

The Tafel plot (Figure S6b) gives a J_{lim} of 10 $mAcm^{-2}$ which corresponds well with reported values in literature for this system.[37] Using this value in Equation 3 gives a value for the diffusion coefficient of 6.23 $x10^{-6}$ cm^2s^{-1} matching the value reported by Kavan et. al.[37] The electrochemical stability of the GNP ink catalyst was compared with that of the sputtered platinum by performing fast cyclic voltammetry scanning followed by EIS measurement, this was repeated ten times and the resulting plots are presented in Figure S7. Neither the sputtered platinum nor the GNP ink catalysts show any change in Rct, indicating that they have some electrochemical stability. This is in contrast to the work of Kavan et al[37] where the thermally deposited platinum catalyst degraded significantly under the same test conditions. It is hypothesized this was due to the different methods of platinum deposition.

DSCs made using the GNP ink, T_{550} = 75 %, show comparable JV characteristics to otherwise identical devices where a platinum catalyst is used, (Table S2 and Figure 5a) and a photo conversion efficiency (PCE) of 6.3% at a V_{max} of 0.68 V is demonstrated. Cells with GNP powder as the catalyst have lower V_{oc} and shunt resistance (500 Ω/cm^2) compared to the shunt resistance of the platinum and ink catalysts (> 3kΩ /cm^2), this is attributed to recombination at the working electrode caused by migration of un-adhered GNP particles across the cell.

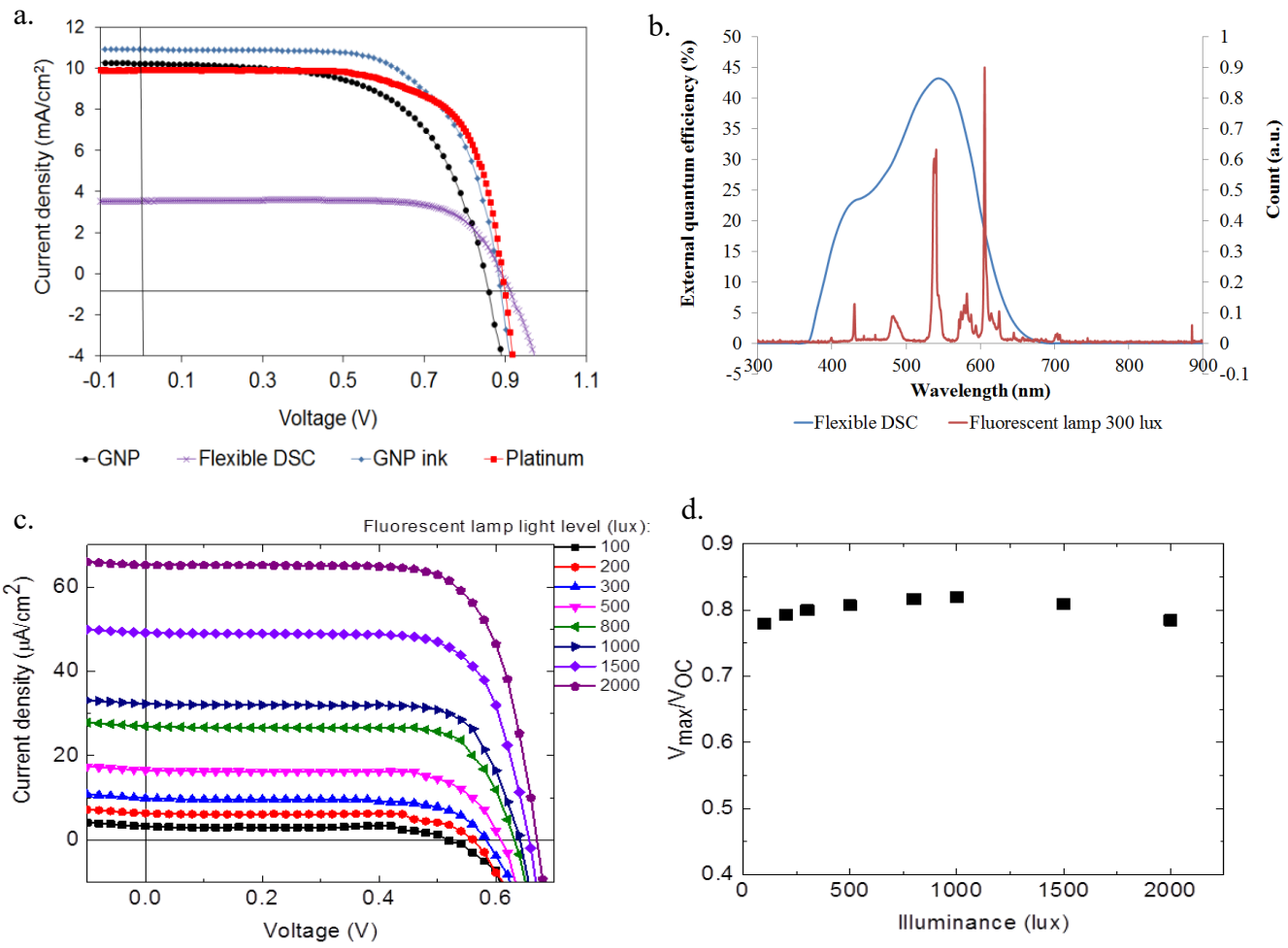

Figure 5(a) Comparison of GNP powder, GNP ink, sputtered platinum catalysts and a flexible DSC with GNP ink catalyst, best performing cells, tested at AM1.5, 1000W/m^{-2}. **(b)** Comparison of flexible DSC EQE spectra with the fluorescent lamp emission spectra. **(c)** DSC performance characteristics of a flexible DSC under a fluorescent lamp. **(d)** V_{max} / V_{oc} ratio under different illumination conditions.

Table 2 – DSC Performance characteristics comparing different catalysts, average and standard deviation (sd) of three results. Individual DSC characteristics are given in Table S2.

Catalyst	V_{oc} (V)		J_{sc} (mA/cm^2)		FF (%)		PCE (%)	
	Average	sd	Average	sd	Average	sd	Average	sd
GNP ink	0.88	0.01	9.06	0.92	64.2	4.4	5.1	0.9
GNP powder	0.85	0.00	8.97	1.24	59.3	1.4	4.5	0.7
Platinum	0.86	0.03	9.32	1.04	63.2	2.6	5.1	0.8
GNP ink flexible cell	0.88	0.00	3.13	0.71	74.6	0.4	2.1	0.5

To make the flexible cell the GNP ink was deposited onto an ITO/PET substrate using K-bar coating, the loading of GNP ink was reduced to T_{550} = 85 % to maximise the photocurrent under reverse illumination. The FTO glass working electrode was replaced with a flexible titanium substrate to create a flexible DSC, which had a maximum PCE of over 2.3 % and an operating voltage of 0.72 V in 1 sun, 1000W/m^{-2} AM1.5 conditions. Since metal based cells must be reverse illuminated through the ITO/PET, catalyst and electrolyte, the intensity of the incoming illumination is reduced and the cells have lower currents compared with forward illuminated glass based devices. The EQE of the metal device is shown in Figure 5b and the wavelength response is favourable to the fluorescent lamp output. The flexible cell was tested from 100 to 2000 lux and the corresponding device performance is shown in Figure 5c and Table S3. In general PCE significantly improved, compared to 1 sun condition, reaching 6 %. At 800 lux, the flexible DSC showed a maximum PCE of 6.0 %. The high shunt resistance of the metal cell (3.7 kΩ/cm^2) is comparable to that of a glass based cell with platinum electrode and is sufficient to ensure high fill factors even at the very low currents achieved under fluorescent lamp illumination. Figure 5d plots the V_{max} to V_{oc} ratio under fluorescent illumination and

the small variation (less than 10 %) demonstrates that the cells are suitable for tracking maximum power point (MPP) using the fractional-voltage method which has been shown to be a method for MPP tracking with low power utilisation[64], suitable for low light applications.

The cobalt electrolyte / dye system is not optimised for reverse illumination and it is expected that by tailoring the dye and the electrolyte compositions photocurrents under both AM1.5 and fluorescent lighting can be improved.

4. Conclusions

This work has developed and characterised a semi-transparent GNP ink with surface area ~400 m^2/g which can be dried at 110ºC enabling deposition onto flexible plastic substrates suitable for roll to roll production. Surface area of the ink does not decrease linearly with the addition of binder material but rather decreases with the addition of a small amount of binder and then plateaus before reducing to almost zero when the GNP content drops below 80 %. Using a dual solvent system enables the viscosity of the ink to be optimised whilst maintaining GNP content and transparency of the deposited ink. By tailoring catalyst performance to the DSC application, the cost and performance of the catalyst can be optimised. The GNP ink has good mechanical integrity and comparable electro-catalytic performance to a sputtered platinum catalyst when used with a cobalt electrolyte, with a PCE of 6.3 % and a V_{oc} of 0.89 V at one sun. The GNP ink was used in a flexible DSC with cobalt electrolyte and and achieved a V_{oc} of 0.89 V and PCE of 2.35 % at 1 sun. At 800 lux the flexible cell, without optimisation demonstrated a PCE of > 6 % indicating great potential for indoor applications with further optimisation.

5. References

[1] Espinosa, N., Hösel, M., Angmo, D., Krebs, F. C. Solar Cells with One-Day Energy Payback for the Factories of the Future. *Energy & Environmental Science* **2012**, *5* (1), 5117.

[2] Sherwani, A. F., Usmani, J. A., Varun. Life Cycle Assessment of Solar PV Based Electricity Generation Systems: A Review. *Renewable and Sustainable Energy Reviews* **2010**, *14* (1), 540–544.

[3] GCELL. http://gcell.com/shop http://gcell.com/shop (accessed Mar 2, 2016).

[4] Harikisun, R., Desilvestro, H. Long-Term Stability of Dye Solar Cells. *Solar Energy* **2011**, *85* (6), 1179–1188.

[5] De Rossi, F., Pontecorvo, T., Brown, T. M. Characterization of Photovoltaic Devices for Indoor Light Harvesting and Customization of Flexible Dye Solar Cells to Deliver Superior Efficiency under Artificial Lighting. *Applied Energy* **2015**, *156*, 413–422.

[6] Ahmad, J., Bazaka, K., Anderson, L. J., White, R. D., Jacob, M. V. Materials and Methods for Encapsulation of OPV: A Review. *Renewable and Sustainable Energy Reviews* **2013**, *27*, 104–117.

[7] Gorlatova, M., Kinget, P., Kymissis, I., Rubenstein, D., Wang, X., Zussman, G. Energy Harvesting Active Networked Tags (EnHANTs) for Ubiquitous Object Networking. *IEEE Wireless Communications* **2010**, *17* (6), 18–25.

[8] Matiko, J. W., Grabham, N. J., Beeby, S. P., Tudor, M. J. Review of the Application of Energy Harvesting in Buildings. *Measurement Science & Technology* **2014**, *25* (1), 12002.

[9] O'Regan, B., Grätzel, M. A Low-Cost, High-Efficiency Solar Cell Based on Dye-Sensitized Colloidal TiO2 Films. *Nature* **1991**, *353* (6346), 737–740.

[10] Ito, S., Murakami, T. N., Comte, P., Liska, P., Grätzel, C., Nazeeruddin, M. K., Grätzel, M. Fabrication of Thin Film Dye Sensitized Solar Cells with Solar to Electric Power Conversion

Efficiency over 10%. *Thin Solid Films* **2008**, *516* (14), 4613–4619.

[11] Wang, M., Anghel, A. M., Marsan, B., Ha, N. L. C., Pootrakulchote, N., Zakeeruddin, S. M., Grätzel, M. CoS Supersedes Pt as Efficient Electrocatalyst for Triiodide Reduction in Dye-Sensitized Solar Cells. *Journal of the American Chemical Society* **2009**, *131* (44), 15976–15977.

[12] Baker, J., McGettrick, J. D., Gethin, D. T., Watson, T. M. Impedance Characteristics of Transparent GNP-Pt Ink Catalysts for Flexible Dye Sensitized Solar Cells. *Journal of the Electrochemical Society* **2015**, *162* (8), H564–H569.

[13] Boschloo, G., Hagfeldt, A. Characteristics of the Iodide/triiodide Redox Mediator in Dye-Sensitized Solar Cells. *Accounts of Chemical Research* **2009**, *42* (11), 1819–1826.

[14] Yella, A., Lee, H.-W., Tsao, H. N., Yi, C., Chandiran, A. K., Nazeeruddin, M. K., Diau, E. W.-G., Yeh, C.-Y., Zakeeruddin, S. M., Gratzel, M. Porphyrin-Sensitized Solar Cells with Cobalt (II/III)-Based Redox Electrolyte Exceed 12 Percent Efficiency. *Science* **2011**, *334* (6056), 629–634.

[15] Peter, L. M. Characterization and Modeling of Dye-Sensitized Solar Cells. **2007**, 6601–6612.

[16] Feldt, S. M., Gibson, E. A., Wang, G., Fabregat, G., Boschloo, G., Hagfeldt, A. Carbon Counter Electrodes Efficient Catalysts for the Reduction of Co(III) in Cobalt Mediated Dye-Sensitized Solar Cells. *Polyhedron* **2014**, *82*, 154–157.

[17] Simon Mathew, Aswani Yella, Peng Gao, Robin Humphry-Baker, Basile F. E. Curchod, Negar Ashari-Astani, Ivano Tavernelli, Ursula Rothlisberger, M. K. N. & M. G. Dye-Sensitized Solar Cells with 13% Efficiency Achieved through the Molecular Engineering of Porphyrin Sensitizers. *Nature Chemistry* **2014**, *6*, 242–247.

[18] Yun, S., Wu, M., Wang, Y., Shi, J., Lin, X., Hagfeldt, A., Ma, T. Pt-like Behavior of High-Performance Counter Electrodes Prepared from Binary Tantalum Compounds Showing High Electrocatalytic Activity for Dye-Sensitized Solar Cells. *ChemSusChem* **2013**, *6* (3), 411–416.

[19] Yun, S., Zhang, H., Pu, H., Chen, J., Hagfeldt, A., Ma, T. Metal Oxide/carbide/carbon

Nanocomposites: In Situ Synthesis, Characterization, Calculation, and Their Application as an Efficient Counter Electrode Catalyst for Dye-Sensitized Solar Cells. *Advanced Energy Materials* **2013**, *3* (11), 1407–1412.

[20] Wu, M., Lin, X., Wang, Y., Wang, L., Guo, W., Qi, D., Peng, X., Hagfeldt, A., Grätzel, M., Ma, T. Economical Pt-Free Catalysts for Counter Electrodes of Dye-Sensitized Solar Cells. *Journal of the American Chemical Society* **2012**, *134* (7), 3419–3428.

[21] Yun, S., Pu, H., Chen, J., Hagfeldt, A., Ma, T. Enhanced Performance of Supported HfO2 Counter Electrodes for Redox Couples Used in Dye-Sensitized Solar Cells. *ChemSusChem* **2014**, *7* (2), 442–450.

[22] Yun, S., Freitas, J. N., Nogueira, A. F., Wang, Y., Ahmad, S., Wang, Z.-S. Dye-Sensitized Solar Cells Employing Polymers. *Progress in Polymer Science* **2015**, (59), 1-40.

[23] Yun, S., Hagfeldt, A., Ma, T. Pt-Free Counter Electrode for Dye-Sensitized Solar Cells with High Efficiency. *Advanced Materials* **2014**, *26* (36), 6210–6237.

[24] Ahmad, S., Bessho, T., Kessler, F., Baranoff, E., Frey, J., Yi, C., Grätzel, M., Nazeeruddin, M. K. A New Generation of Platinum and Iodine Free Efficient Dye-Sensitized Solar Cells. *Physical Chemistry Chemical Physics* **2012**, *14* (30), 10631.

[25] Ahmad, S., Guillén, E., Kavan, L., Grätzel, M., Nazeeruddin, M. K. Metal Free Sensitizer and Catalyst for Dye Sensitized Solar Cells. *Energy & Environmental Science* **2013**, *6* (207890), 3439–3466.

[26] Kay, A., Grätzel, M. Low Cost Photovoltaic Modules Based on Dye Sensitized Nanocrystalline Titanium Dioxide and Carbon Powder. *Solar Energy Materials and Solar Cells* **1996**, *44* (1), 99–117.

[27] Lee, W. J., Ramasamy, E., Lee, D. Y., Song, J. S. Performance Variation of Carbon Counter Electrode Based Dye-Sensitized Solar Cell. *Solar Energy Materials and Solar Cells* **2008**, *92* (7), 814–818.

[28] Baker, J., Deganello, D., Gethin, D. T., Watson, T. M. Flexographic Printing of Graphene Nanoplatelet Ink to Replace Platinum as Counter Electrode Catalyst in Flexible Dye Sensitised Solar Cell. *Materials Research Innovations* **2014**, *18* (2), 86–90.

[29] Roy-mayhew, J. D., Aksay, I. A. Graphene Materials and Their Use in Dye-Sensitized Solar Cells. *Chemical Reviews* **2014**, *114*, 6323–6348.

[30] Imoto, K., Takahashi, K., Yamaguchi, T., Komura, T., Nakamura, J. I., Murata, K. High-Performance Carbon Counter Electrode for Dye-Sensitized Solar Cells. *Solar Energy Materials and Solar Cells* **2003**, *79* (4), 459–469.

[31] Dodoo-arhin, D., Howe, R. C. T., Hu, G., Zhang, Y., Hiralal, P., Bello, A., Amaratunga, G., Hasan, T., Hu, G., Zhang, Y., Hiralal, P., Bello, A., Hasan, T. Inkjet-Printed Graphene Electrodes for Dye-Sensitized Solar Cells. *Carbon* **2016**, *105*, 33–41.

[32] Yin, Z., Zhu, J., He, Q., Cao, X., Tan, C., Chen, H., Yan, Q., Zhang, H. Graphene-Based Materials for Solar Cell Applications. *Advanced Energy Materials* **2014**, *4* (1), 1–19.

[33] Casaluci, S., Gemmi, M., Pellegrini, V., Di Carlo, A., Bonaccorso, F. Graphene-Based Large Area Dye-Sensitized Solar Cell Module. *Nanoscale* **2016**.

[34] Yun, S., Liu, Y., Zhang, T., Ahmad, S. Recent Advances in Alternative Counter Electrode Materials for Co-Mediated Dye-Sensitized Solar Cells. *Nanoscale* **2015**, *7*, 11877–11893.

[35] Baker, J., Watson, T. M., Jones, D., Deganello, D., Gethin, D. T., Claypole, T. C. Optically Transparent Graphene Nanoplatelet Inks as Low Cost Electrocatalysts for Liquid Dye Sensitised Solar Cells. *MRS Proceedings* **2014**, *1667*.

[36] Roy-Mayhew, J. D., Boschloo, G., Hagfeldt, A., Aksay, I. A. Functionalized Graphene Sheets as a Versatile Replacement for Platinum in Dye-Sensitized Solar Cells. *ACS Applied Materials and Interfaces* **2012**, *4* (5), 2794–2800.

[37] Kavan, L., Yum, J.-H., Graetzel, M. Optically Transparent Cathode for Co(III/II) Mediated Dye-Sensitized Solar Cells Based on Graphene Oxide. *ACS applied materials & interfaces* **2012**,

4 (12), 6999–7006.

[38] Kavan, L., Yum, J. H., Grätzel, M. Graphene Nanoplatelets Outperforming Platinum as the Electrocatalyst in Co-Bipyridine-Mediated Dye-Sensitized Solar Cells. *Nano Letters* **2011**, *11* (12), 5501–5506.

[39] Kavan, L., Liska, P., Zakeeruddin, S. M., Grätzel, M. Low-Temperature Fabrication of Highly-Efficient, Optically-Transparent (FTO-Free) Graphene Cathode for Co-Mediated Dye-Sensitized Solar Cells with Acetonitrile-Free Electrolyte Solution. *Electrochimica Acta* **2016**, *195*, 34–42.

[40] Asghar, M. I., Miettunen, K., Halme, J., Vahermaa, P., Toivola, M., Aitola, K., Lund, P. Review of Stability for Advanced Dye Solar Cells. *Energy & Environmental Science* **2010**, *3* (4), 418.

[41] Yun, S., Lund, P. D., Hinsch, A. Stability Assessment of Alternative Platinum Free Counter Electrodes for Dye-Sensitized Solar Cells. *Energy Environ. Sci.* **2015**, *8* (12), 3495–3514.

[42] Miettunen, K., Toivola, M., Hashmi, G., Salpakari, J., Asghar, I., Lund, P. A Carbon Gel Catalyst Layer for the Roll-to-Roll Production of Dye Solar Cells. *Carbon* **2011**, *49* (2), 528–532.

[43] Toivola, M., Halme, J., Miettunen, K., Aitola, K., Lund, P. D. Nanostructured Dye Solar Cells on Flexible Substrates-Review. *International Journal of Energy Research* **2009**, *33* (13), 1145–1160.

[44] Watson, T., Reynolds, G., Wragg, D., Williams, G., Worsley, D. Corrosion Monitoring of Flexible Metallic Substrates for Dye-Sensitized Solar Cells. *International Journal of Photoenergy* **2013**, *2013*, 9–11.

[45] Watson, T. M., Reynolds, G. J., Worsley, D. A. Painted Steel Mounted Dye Sensitised Solar Cells: Titanium Metallisation Using Magnetron Sputtering. *Ironmaking & Steelmaking* **2011**, *38* (3), 168–172.

[46] Reynolds, G. J., Watson, T. M., Williams, G., Worsley, D. Corrosion Resistance of Metallic

Substrates for the Fabrication Dye-Sensitized Solar. *ECS Transactions* **2011**, *33* (17).

[47] Miettunen, K., Ruan, X., Saukkonen, T., Halme, J., Toivola, M., Guangsheng, H., Lund, P. Stability of Dye Solar Cells with Photoelectrode on Metal Substrates. *Journal of The Electrochemical Society* **2010**, *157* (6), B814.

[48] Ito, S., Ha, N.-L. C., Rothenberger, G., Liska, P., Comte, P., Zakeeruddin, S. M., Péchy, P., Nazeeruddin, M. K., Grätzel, M. High-Efficiency (7.2%) Flexible Dye-Sensitized Solar Cells with Ti-Metal Substrate for Nanocrystalline-TiO2 Photoanode. *Chemical communications (Cambridge, England)* **2006**, No. 38, 4004–4006.

[49] Roy-mayhew, J. D., Pope, M. A., Punckt, C., Aksay, I. A. Intrinsic Catalytic Activity of Graphene Defects for the Co. *Applied Materials and Interfaces* **2016**.

[50] Zhang, D. W., Li, X. D., Li, H. B., Chen, S., Sun, Z., Yin, X. J., Huang, S. M. Graphene-Based Counter Electrode for Dye-Sensitized Solar Cells. *Carbon* **2011**, *49* (15), 5382–5388.

[51] Kavan, L., Yum, J., Graetzel, M. Optically Transparent Cathode for Co (III / II) Mediated Dye-Sensitized Solar Cells Based on Graphene Oxide. **2012**.

[52] Kavan, L., Yum, J. H., Gratzel, M. Optically Transparent Cathode for Dye-Solar Cells Based on Graphene Nanoplatelets. *ACS nano* **2011**, *5* (1), 165–172.

[53] Bacon, G. . The Interlayer Spacing of Graphite. *Acta Crystallographica* **1951**, *4* (6), 558–561.

[54] Hernandez, Y., Nicolosi, V., Lotya, M., Blighe, F. M., Sun, Z., De, S., McGovern, I. T., Holland, B., Byrne, M., Gun'Ko, Y. K., Boland, J. J., Niraj, P., Duesberg, G., Krishnamurthy, S., Goodhue, R., Hutchison, J., Scardaci, V., Ferrari, A. C., Coleman, J. N. High-Yield Production of Graphene by Liquid-Phase Exfoliation of Graphite. *Nature nanotechnology* **2008**, *3* (9), 563–568.

[55] SIGMA ALDRICH. NMP MSDS. 2016, pp 1–19.

[56] SIGMA ALDRICH. MSDS IPA. 2016, pp 1–8.

[57] Korkut, S., Roy-Mayhew, J. D., Dabbs, D. M., Milius, D. L., Aksay, I. a. High Surface Area

Tapes Produced with Functionalized Graphene. *ACS Nano* **2011**, *5* (6), 5214–5222.

[58] Kavan, L., Yum, J. H., Graetzel, M. Graphene-Based Cathodes for Liquid-Junction Dye Sensitized Solar Cells: Electrocatalytic and Mass Transport Effects. *Electrochimica Acta* **2014**, *128*, 349–359.

[59] Gong, J., Zhou, Z., Sumathy, K., Yang, H., Qiao, Q. Activated Graphene Nanoplatelets as a Counter Electrode for Dye-Sensitized Solar Cells. *Journal of Applied Physics* **2016**, *119* (13).

[60] Rouquerolt, J., Avnir, D., Fairbridge, C. W., Everett, D. H., Haynes, J. H., Pernicone, N., Ramsay, J. D. F., Sing, K. S. W., Unger, K. K. Recommendations for the Characterization of Porous Solids. *Pure and Applied Chemistry* **1994**, *66* (8), 1739–1758.

[61] Kwon, W., Kim, J.-M., Rhee, S.-W. A New Equivalent Circuit Model for Porous Carbon Electrodes in Charge Transfer Reaction of Iodide/triiodide Redox Couples. *Electrochimica Acta* **2012**, *68*, 110–113.

[62] Kavan, L., Yum, J. H., Gratzel, M. Optically Transparent Cathode for Dye- Sensitized Solar Cells Based on Graphene Nanoplatelets. *ACS Nano* **2011**, *5* (1), 165–172.

[63] Raistrick, I., MacDonald, J., Franceschetti, A. *Theory of Impedance Spectroscopy*; MacDonald, J., Ed.; Wiley, John, 1987.

[64] Lee, H. K. H., Li, Z., Durrant, J. R., Tsoi, W. C. Is Organic Photovoltaics Promising for Indoor Applications? *Applied Physics Letters* **2016**, *108* (25), 253301.

ASSOCIATED CONTENT

Supporting Information. Examples of slot die coating, flexographic printing and K-bar coating, AFM analysis of GNPs, EIS of CMC, and EQE of the flexible DSC are given in the supporting information. This material is available free of charge via the Internet at http://pubs.acs.org.

AUTHOR INFORMATION

Corresponding Author *T.M.Watson@swansea.ac.uk, SPECIFIC, College of Engineering, Swansea University Bay Campus, Swansea SA1 8EN.

This manuscript was written through contributions of all authors. All authors have given approval to the final version of the manuscript.

ACKNOWLEDGMENT

This work was part-funded by the European Social Fund (ESF) and Haydale Ltd., through the European Union's Convergence programme administered by the Welsh Government. Materials provided by Haydale Ltd. The authors would like to thank the EPSRC and TSB for supporting this work through the SPECIFIC Innovation and Knowledge Centre, EPSRC Supersolar, EP/5017361/1 (JB). We are very grateful to Ser Cymru funding from the Welsh Assembly Government (K.H.L / W.C.T.)"

Table of Contents

This work develops a GNP ink of high surface area which can be printed using roll to roll technologies to produce a semi-transparent catalyst. Post deposition the ink needs only a 110ºC drying step enabling the use of plastic substrates. Flexible dye sensitised solar cells suitable for indoor applications were produced with efficiencies of over 6.0 %.